

Formation of Anomalously Energetic Ions in Hollow Cathode Plume by Charge Separation Instability

Yinjian Zhao, Baisheng Wang, and Tianhang Meng*

School of Energy Science and Engineering, Harbin Institute of Technology, Harbin 150001, People's Republic of China

(Dated: January 13, 2025)

Hollow cathodes are becoming the bottleneck of many electric propulsion systems, because of the sputtering and erosion on both cathodes and thrusters from the generation of anomalously energetic ions. So far, it is believed that energetic ions are formed by waves and instabilities always accompanied in cathode discharge, but there is no evidence yet that those proposed instabilities can lead to such high ion energies measured in experiments. In this work, a new mechanism of charge separation instability in hollow cathode plume is found via fully kinetic PIC simulations, which can easily produce energetic ions to the same level as measured in experiments.

A steady working hollow cathode is crucial for coupling with many types of electric propulsion thrusters, but hollow cathodes seldom or never operate without oscillations over a broad band of frequency, along with the generation of anomalously energetic ions causing sputtering and erosion on both cathodes and thrusters. For example, the cathode life of the early prototype of SPT-100 Hall thrusters had difficulties to reach the 8000 hours lifetime requirement [1]; the PPS-1350 thruster was found to have a more serious asymmetric erosion of the ceramic channel on the cathode side [2]; in more recent HERMeS thruster tests, it was also found that the erosion rate is very sensitive to the cathode position [3]. Therefore, as great progress has been made on thruster performance and stability, hollow cathodes are becoming the bottleneck that restricts further improvements of electric propulsion systems.

The phenomenon that hollow cathodes can produce ions with energies significantly in excess of the discharge voltage has been found experimentally since 1990s [4]. Theories have been proposed to explain these energetic ions, such as the (DC) potential hill model [5] and the ion acoustic turbulence (IAT) model [6, 7]. Since experimental measurements of the potential distributions could not find a DC potential hill responsible for such energetic ions (> 50 eV) [8], but the existence of ion acoustic waves has been confirmed in experiments [9], the IAT theory became dominant. However, as with more and more reports witnessing the presence of energetic ions under scarce or undetectable ion acoustic waves, there seem to be other mechanisms that can contribute to the existence of such ions. Especially when it comes to the physical picture of the IAT, as pointed out by D.M. Goebel et al. [10], the link between waves and the increase of the ion energy still lacks an explanation, and there is no evidence yet that IAT alone can lead to such high ion energies.

From the perspective of numerical simulations on the cathode instabilities, fluid models are mainly applied in the channel, where the plasma density is high and assumed near equilibrium, such as zero-dimensional (0D)

models [11] and 1D models [12] for estimating plasma production and temperature, and 2D models [6, 13] using the Richardson-Dushman equation, which can better describe the plasma-wall interaction and neutral flow effects. There are also hybrid models [14] representing electrons as fluid and ions as particles, resulting in favorable comparisons with some experiments. In order to simulate the cathode plume, where the plasma density becomes low, kinetic approaches are needed. Pioneers of D. Levko et al. [15] carried out 2D Cartesian fully kinetic particle-in-cell (PIC) simulations on a miniaturized orificed hollow cathode, and Cao et al. [16, 17] established a 2D-RZ cylindrical PIC model, both of which found non-Maxwellian behavior for electron and ion velocity distributions in the plume. In addition, K. Hara et al. [18] used a 1D Vlasov solver to study the ion acoustic turbulence relevant to hollow cathodes.

In order to investigate the instabilities and energetic ions occurred in the cathode plume, kinetic models are preferred than fluid models. While Vlasov solvers are usually limited in low dimensions due to large computations, carrying out fully kinetic PIC simulations without speed-up tricks that may bring in non-physical effects is also challenging. Note that D. Levko et al. [15] and Cao et al. [16, 17] both applied speed-up tricks in their PIC models, such as reducing the ion mass, increasing the vacuum permittivity, or decreasing the simulated cathode size. These speed-up tricks are known to potentially introduce inaccurate results in Hall thruster azimuthal instability simulations. For example, the two 2D classic benchmark works did not apply any of these speed-up tricks [19, 20], but attempted to use more parallel computing techniques to accelerate the simulations. Because in the area of Hall thruster simulations, a great amount of efforts have been devoted to even carry out massive 3D PIC simulations [21, 22], it is surprising that PIC simulations on hollow cathodes have not been pushed anywhere close to the limit of nowadays supercomputing power, taking advantages of well parallelized PIC codes.

Therefore, in this work, we attempt to simulate the cathode plume using the fully kinetic PIC method in 2D-RZ geometry without any speed-up tricks up to the centimeter scale and tens of microseconds, in order to

* mength@hit.edu.cn

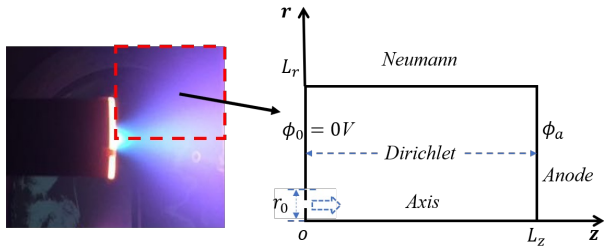


FIG. 1. A photo of a hollow cathode discharge [25] (left) and 2D-RZ simulation setup (right).

be capable of revealing more underlying physics with respect to the hollow cathode instabilities and energetic ions. The well parallelized PIC code WarpX [23] is applied in this work to carry out relatively large-scale electrostatic PIC simulations. Instead of the ion acoustic turbulence, which would be considered as developed from a 1st order instability, significant 0th order instabilities are observed in this work, accompanied with strong oscillating potentials due to charge non-neutrality. We therefore would like to call it the charge separation instability/turbulence, occurred for example in astrophysical plasmas too [24]. The simulation results indicate that energetic ions can be very easily generated during the evolution of the charge separation instability.

The simulation setup is described as follows. The chosen simulation geometry and domain are illustrated in Fig.1, which is a 2D-RZ cylindrical region with size 1.024×1.024 cm, ranging from the cathode exit to the anode plate. The Dirichlet condition is applied on the cathode and anode boundaries with $\phi_c = 0$ V and $\phi_a = 20$ V, respectively. The Neumann condition $\partial\phi/\partial r = 0$ is applied on the maximum r boundary. All these three boundaries are set to be absorbing for particles. At the beginning of the simulation, electrons and ions start to be injected from the keeper orifice with radius $r_0 = 0.5$ mm. Electrons and ions are sampled according to Maxwellian velocity distributions with temperatures $T_e = 5$ eV, $T_i = 0.5$ eV, and drifting velocities v_{de} , v_{di} , respectively. The corresponding thermal velocities are $v_{te} \approx 9.4 \times 10^5$ m/s for electrons, and $v_{ti} \approx 600$ m/s for the chosen xenon ions. Electrons and ions are assumed to have the same number density at injection $n_0 = 10^{18}$ m⁻³, and the electron current is set to be $I_0 = 0.5$ A, thus the electron drifting velocity can be computed as $v_{de} = I_0/(en_0\pi r_0^2) \approx 7.9 \times 10^6$ m/s, where e is the elementary charge, and $v_{di} = 1000$ m/s is chosen empirically. Based on n_0 and T_e , the Debye length is $\lambda_D \approx 1.66 \times 10^{-5}$ m, such that the cell sizes are chosen to be $\Delta r = \Delta z = 10^{-5}$ m, resulting in $N_r \times N_z = 1024 \times 1024$ cells. The time step is set to be $\Delta t = 0.2\omega_{pe} \approx 3.55 \times 10^{-12}$ s. Therefore, to reach a steady state in a few μ s, more than 10^6

time steps are needed. The number of particles injected per time step (the same for electrons and ions) is chosen to be $N_p = 400$, which results in the macro-particle weight $w_0 = I_0\Delta t/(eN_p) \approx 27700$, which is set to be a constant for all macro-particles. The Monte Carlo collision (MCC) model that accounts for the electron-neutral elastic, excitation, and ionization collisions is considered, with a fixed Xenon atom density distribution, $n_a = n_{a0}/[(r^2 + z^2)^{1/2} + 1]^2$, where the atom density at the cathode exit is set to be $n_{a0} = 10^{19}$ m⁻³, and the atom temperature is 0.5 eV. This simulation is carried out using 256 MPI ranks on a single computing node with two AMD EPYC 9754 CPUs. The run time is about 3.39 days to finish 5×10^6 time steps, i.e., 17.75 μ s.

The evolution of the charge separation instability is captured by the simulation as presented in Fig.2. (1) At the very beginning, at time step $t = 10^4$ (≈ 35.5 ns), shown in the first row of Fig.2, electrons are injected and can travel to the anode, while expanding axially and radially, such that the electron density n_e drops quickly. Because ions are slow and impeded by the anode potential, an electron and ion charge separation is formed and a negative potential (~ -100 V) is established by those extracted electrons near the cathode exit, shown in the potential ϕ plot. Looking at the z - v_{iz} plot, there are two groups of ions, one occupies the whole plume region with a low density n_i , which are those newly ionized ions; ions in the other group are extracted and gain high velocities up to $v_{iz} \approx 12500$ m/s near the cathode exit, which are pulled by electrons and try to retrieve the neutrality. (2) As shown in the second row of Fig.2 at $t = 10^5$ (≈ 0.355 μ s), as more ions are extracted by the electrons, a relatively high potential region (~ -30 V) is formed at $z \approx 0.1$ cm near the axis, which is located in between of two low potential regions, a small one on the left and a big one on the right. Looking at the z - v_{iz} plot, when $z < 0.1$ cm, some high speed ions are decelerated due to the rise of the local potential, and when $z > 0.1$ cm, some ions are accelerated due to the drop of the local potential. The opposite is found in the z - v_{ez} plot for some electrons, where they are accelerated at $z < 0.1$ cm and decelerated at $z > 0.1$ cm. (3) Then, there are more extracted ions to form a higher potential region (~ 150 V), as shown in the third row of Fig.2 at $t = 2.2 \times 10^5$ (≈ 0.781 μ s). The previous small low potential region on the left grows big too, which is a newly formed group of electrons, that help to extract injected ions and impede injected electrons, such that some electrons cannot be extracted and may return back to the cathode, as shown by the vortex near the cathode in the z - v_{ez} plot. Looking at the n_e plot, we can see two high-density branches in the plume, indicating the discontinuity of electron extraction. (4) The above process reaches a steady-state after about 2 μ s, which can be seen from the average density and energy plots in Fig.3, but the charge separation instability remains, causing the continuous formation of the alternating high and low potential regions, which propagate towards the anode along with groups of non-neutral elec-

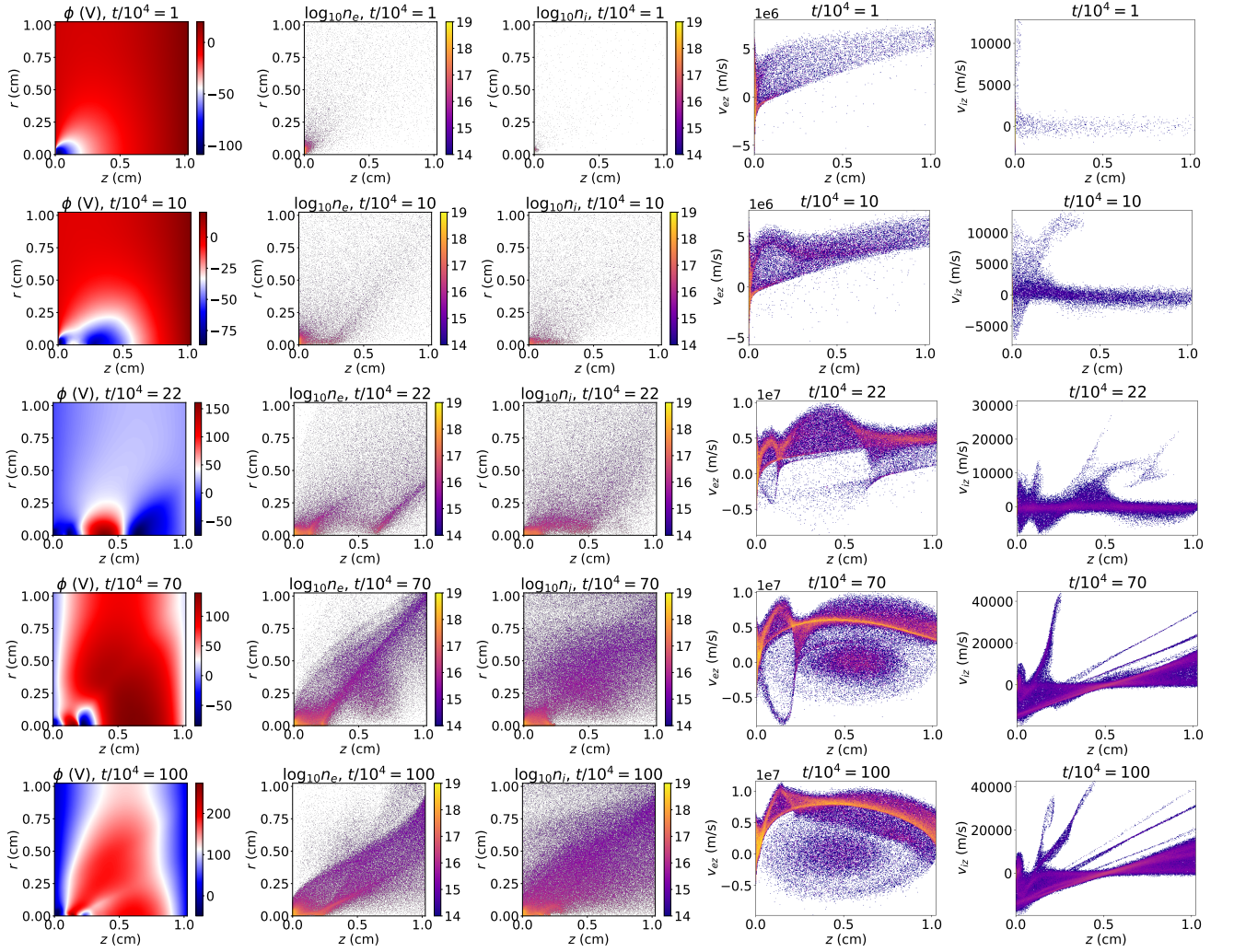


FIG. 2. The time evolution of the charge separation instability illustrated by the distributions of potential ϕ , electron density n_e (m^{-3}), ion density n_i (m^{-3}), electron and ion z - v_z phase space plots, at different time steps t .

trons or ions, as shown by the last two rows of Fig.2 at time $t = 7 \times 10^5$ ($\approx 2.485 \mu s$) and $t = 10^6$ ($\approx 3.55 \mu s$). From the two z - v_{ez} plots, we can see that the center round-shape electrons are due to ionization, while those with much higher energy are mostly formed and driven by the charge separation instability. From the two z - v_{iz} plots, we can see that after gaining a significant amount of energy, ions are gradually decelerated towards the anode as branches one after another. Those low energy ions in the middle of the plot are mostly generated by ionization, and some may move to the anode, while others may return back to the cathode.

As mentioned earlier, the convergence of the simulation can be seen in the average density and energy plots over time, as shown in Fig.3. In order to verify that the number of macro-particles applied is large enough, two corresponding tests are run with reduced $N_p = 200$ and 100, and their average density and energy results are also plotted along with the curves of the base case with $N_p = 400$. As we can see from the figures, the results

match with each other very well. At the steady state, the average ion density in the plume is about $2.8 \times 10^{15} m^{-3}$, and the electron density is about $1 \times 10^{15} m^{-3}$. The average ion kinetic energy is about 25 eV, and that for electrons is about 140 eV. In addition, oscillations are observed in these average density and energy plots. To better analyze these oscillations, and to be more related to diagnostic approaches in experiments, the number of macro-particles reaching the anode plane is recorded and computed to obtain the anode current, shown in Fig.3, along with a dashed smoothed curve to indicate the oscillation period and frequency. By simply counting the number of oscillation peaks between a certain time range, an oscillation with period $1.25 \mu s$ and frequency 0.8 MHz can be detected. Further more, FFT is done on the anode current data, and the plot in the MHz scale shows the 0.8 MHz wave with an amplitude about 20 mA, as well as a 4 MHz wave with an amplitude about 10 mA. These MHz oscillations have been found in experiments too, such as Fig.12 in [26] and Fig.15 in [8]. In the GHz

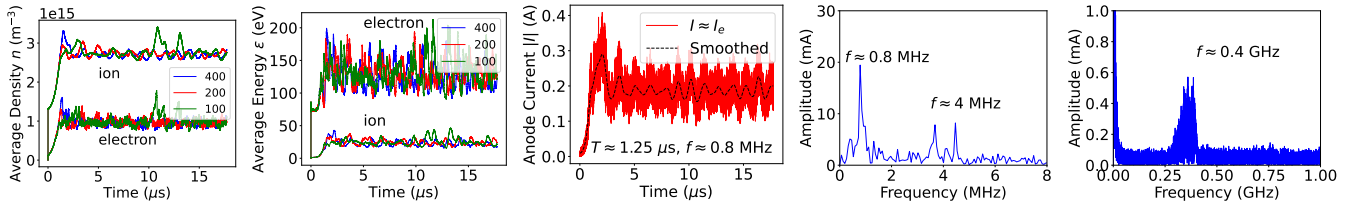


FIG. 3. From the left to the right: the average density and energy over time; the anode current oscillation over time; the spectral plot in the MHz scale; and the spectral plot in the GHz scale.

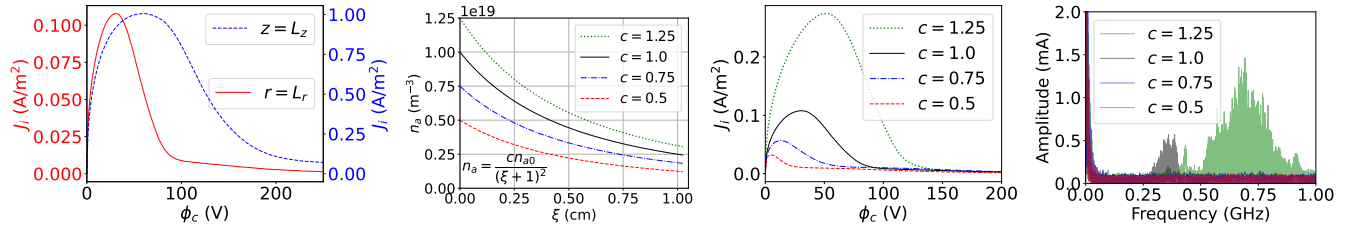


FIG. 4. From left to right: ion current density J_i over collector potential ϕ_c on $r = L_r$ and $z = L_z$ two planes; variation of the neutral atom density distribution n_a , where $\xi^2 = r^2 + z^2$; J_i - ϕ_c on $r = L_r$ plane and the GHz spectral plots of cases varying n_a .

scale, a 0.4 GHz high frequency wave can be detected with small amplitude about 0.6 mA, which was detected too in experiments, such as Fig.10 in [27].

Then, to diagnose energetic ions, we mimic the way of RPA measurements commonly used in experiments. One RPA is considered to be placed on the $r = L_r$ plane, and those ions within the cylindrical shell with radius L_r , thickness $2\Delta r$, and length L_z are taken into account. Similarly, another RPA is placed on the $z = L_z$ plane, and those ions within the cylinder with radius L_r and length $2\Delta z$ are taken into account. Then, the ‘‘collector’’ potential ϕ_c is scanned from 0 to 250 V, and those ions with higher energies (kinetic energy normal to the RPA surface) are counted accumulatively, multiplied by the ion radial/axial velocity, the density, and the unit charge, thus the current density J_i can be obtained as a function of the collector potential ϕ_c . The plot is shown in Fig.4, from which we can see the J_i collected has a very similar profile to many experimental measurements, such as Fig.2 and Fig.5 in [4], Fig.15 and Fig.16 in [28]. Energetic ions (> 50 eV) are easily detected as those in experiments, indicating the easiness of energetic ion generation due to the charge separation instability.

At last, we show that the magnitude of the neutral atom density distribution n_a can greatly affect the generation of energetic ions. Different n_a distributions are considered by varying the constant c in the formula $n_a = cn_{a0}/(\xi+1)^2$, where $\xi^2 = r^2 + z^2$, as shown in Fig.4. The simulation results of the radial current density J_i for different cases are plotted in Fig.4 too, we can see that decreasing n_a leads to lower ion energies collected, which makes sense because as n_a gradually decreases to some

point, the discharge can not be sustained and no more ions can be generated. However, the opposite trend has been found in experiments as well that decreasing n_a can lead to higher ion energies [25]. This contradiction may be explained that those experiments and the simulations in this work are in different regimes, such as high current (a few amperes) in experiments versus only 0.5 A in the simulation for saving computational cost. For the MHz oscillations, although they are affected by n_a , but no obvious trend can be obtained yet. For the GHz oscillations, it can be seen in Fig.4, as n_a decreases GHz oscillations gradually disappear.

In summary, a new mechanism of charge separation instability in hollow cathode plume is found via fully kinetic PIC simulations, which can easily lead to energetic ions and is agreed with experimental measurements in the literature qualitatively. It is believed that this new finding opens up a promising avenue to explain the gap between theories and experiments on the generation of anomalously energetic ions and the long lasting mystery of hollow cathode instabilities. Numerous follow-up works can be carried out, such as more massive simulations with higher currents and larger spatial size, and parametric studies compared to experiments quantitatively.

ACKNOWLEDGMENTS

The authors acknowledge the support from National Natural Science Foundation of China (grant number U22B20120 and 5247120164). This research used the open-source PIC code WarpX we acknowledge all WarpX contributors.

-
- [1] B. Arhipov, A. Bober, R. Gnizdor, K. Kozubsky, A. Korakin, N. Maslennikov, and S. Pridannikov, The results of 7000-hour spt-100 life testing, in *24th International Electric Propulsion Conference* (1995) pp. IEPC-95-39.
- [2] G. Bourgeois, S. Mazouffre, and N. Sadeghi, Unexpected transverse velocity component of x_e^+ ions near the exit plane of a hall thruster, *Physics of Plasmas* **17**, 113502 (2010).
- [3] G. Williams, J. Kamhawi, M. Choi, T. Haag, W. Huang, D. Herman, J. Gilland, and P. Peterson, Wear trends of the hermes thruster as a function of throttle point, in *35th International Electric Propulsion Conference* (2017) pp. IEPC-2017-207.
- [4] V. J. Friedly and P. J. Wilbur, High current hollow cathode phenomena, *Journal of Propulsion and Power* **8**, 635 (1992).
- [5] I. Kameyama and P. Wilbur, Potential-hill model of high-energy ion production near high current hollow cathodes, in *21st International Symposium on Space Technology and Science (Sonic City, Omiya, Japan)*, *ISTS Pap.* (1998) pp. No. 98-a-2-17.
- [6] I. G. Mikellides, I. Katz, D. M. Goebel, and J. E. Polk, Hollow cathode theory and experiment. ii. a two-dimensional theoretical model of the emitter region, *Journal of Applied Physics* **98**, 113303 (2005).
- [7] I. G. Mikellides, I. Katz, D. M. Goebel, and K. K. Jameson, Evidence of nonclassical plasma transport in hollow cathodes for electric propulsion, *Journal of Applied Physics* **101**, 063301 (2007).
- [8] D. M. Goebel, K. K. Jameson, I. Katz, and I. G. Mikellides, Potential fluctuations and energetic ion production in hollow cathode discharges, *Physics of Plasmas* **14**, 103508 (2007).
- [9] B. A. Jorns, C. Dodson, D. M. Goebel, and R. Wirz, Propagation of ion acoustic wave energy in the plume of a high-current lab_6 hollow cathode, *Phys. Rev. E* **96**, 023208 (2017).
- [10] D. M. Goebel, G. Becatti, I. G. Mikellides, and A. Lopez Ortega, Plasma hollow cathodes, *Journal of Applied Physics* **130**, 050902 (2021).
- [11] A. Gurciullo, A. L. Fabris, and T. Potterton, Numerical study of a hollow cathode neutraliser by means of a zero-dimensional plasma model, *Acta Astronautica* **174**, 219 (2020).
- [12] M. Panelli, A. Smoraldi, V. De Simone, and F. Battista, Development and validation of simplified 1d models for hollow cathode analysis and design, *Aerotecnica Missili & Spazio* **97**, 49 (2018).
- [13] I. G. Mikellides, I. Katz, D. M. Goebel, J. E. Polk, and K. K. Jameson, Plasma processes inside dispenser hollow cathodes, *Physics of Plasmas* **13**, 063504 (2006).
- [14] K. Kubota, Y. Oshio, K. Torii, Y. Okuno, H. Watanabe, S. Cho, and I. Funaki, Comparisons between hybrid-pic simulation and plume plasma measurements of lab_6 hollow cathode, in *36th International Electric Propulsion Conference* (2019) pp. IEPC-2019-865.
- [15] D. Levko, Y. P. Bliokh, V. T. Gurovich, and Y. E. Krasik, Instability of plasma plume of micro-hollow cathode discharge, *Physics of Plasmas* **22**, 113502 (2015).
- [16] S. Cao, J. Ren, H. Tang, Z. Zhang, Y. Wang, J. Cao, and Z. Chen, Numerical simulation of plasma power deposition on hollow cathode walls using particle-in-cell and monte carlo collision method, *Physics of Plasmas* **25**, 103512 (2018).
- [17] S. Cao, J. Ren, H. Tang, R. Pan, Z. Zhang, K. Zhang, and J. Cao, Modeling on plasma energy balance and transfer in a hollow cathode, *Journal of Physics D: Applied Physics* **52**, 285202 (2019).
- [18] K. Hara and C. Treece, Ion kinetics and nonlinear saturation of current-driven instabilities relevant to hollow cathode plasmas, *Plasma Sources Science and Technology* **28**, 055013 (2019).
- [19] T. Charoy, J. P. Boeuf, A. Bourdon, J. A. Carlsson, P. Chabert, B. Cuenot, D. Eremin, L. Garrigues, K. Hara, I. D. Kaganovich, A. T. Powis, A. Smolyakov, D. Sydorenko, A. Tavant, O. Vermorel, and W. Villafana, 2d axial-azimuthal particle-in-cell benchmark for low-temperature partially magnetized plasmas, *Plasma Sources Science and Technology* **28**, 105010 (2019).
- [20] W. Villafana, F. Petronio, A. C. Denig, M. J. Jimenez, D. Eremin, L. Garrigues, F. Taccogna, A. Alvarez-Laguna, J. P. Boeuf, A. Bourdon, P. Chabert, T. Charoy, B. Cuenot, K. Hara, F. Pechereau, A. Smolyakov, D. Sydorenko, A. Tavant, and O. Vermorel, 2d radial-azimuthal particle-in-cell benchmark for $e \times b$ discharges, *Plasma Sources Science and Technology* **30**, 075002 (2021).
- [21] L. Xie, X. Luo, Z. Zhou, and Y. Zhao, Effect of plasma initialization on 3d pic simulation of hall thruster azimuthal instability, *Physica Scripta* **99**, 095602 (2024).
- [22] W. Villafana, B. Cuenot, and O. Vermorel, 3d particle-in-cell study of the electron drift instability in a hall thruster using unstructured grids, *Physics of Plasmas* **30**, 033503 (2023).
- [23] L. Fedeli, A. Huebl, F. Boillod-Cerneux, T. Clark, K. Gott, C. Hillairet, S. Jaure, A. Leblanc, R. Lehe, A. Myers, C. Piechurski, M. Sato, N. Zaim, W. Zhang, J.-L. Vay, and H. Vincenti, Pushing the frontier in the design of laser-based electron accelerators with groundbreaking mesh-refined particle-in-cell simulations on exascale-class supercomputers, in *SC22: International Conference for High Performance Computing, Networking, Storage and Analysis* (2022) pp. 1-12.
- [24] S. Koide, Charge separation instability in an unmagnetized disk plasma around a kerr black hole, *Phys. Rev. D* **83**, 023003 (2011).
- [25] F.-F. Wang, T.-H. Meng, D.-R. Yu, Z.-X. Ning, and X.-M. Zhu, Presence of energetic ions in hollow cathode discharge with low frequency oscillations, *Journal of Physics D: Applied Physics* **55**, 455202 (2022).
- [26] A. P. Scott and D. M. Goebel, Hollow cathode discharge instability onset in electric thrusters, *Journal of Applied Physics* **135**, 123301 (2024).
- [27] A. Plokhikh, N. Vazhenin, V. Kim, and S. Baranov, Experimental investigation of the hollow cathode electromagnetic radiation, in *34th International Electric Propulsion Conference* (2015) pp. IEPC-2015-489p.
- [28] R. Thomas, H. Kamhawi, and G. Williams, High current hollow cathode plasma plume measurements, in *33th International Electric Propulsion Conference* (2013) pp. IEPC-2013-076.